

The physical properties of *Fermi* BL Lac objects jets

Dahai Yan, Houdun Zeng, and Li Zhang*

Department of Physics, Yunnan University, Kunming, China

Accepted 2014 January 18. Received 2013 October 27; in original form 2013 January 17.

ABSTRACT

We investigate the physical properties of BL Lac objects (BL Lacs) jets by modeling the quasi-simultaneous spectral energy distributions (SEDs) of 22 *Fermi* BL Lac objects in the frame of a simple one-zone synchrotron self-Compton (SSC) model. We obtained the best-fit model parameters and their uncertainties for each BL Lac object through the χ^2 -minimization procedure and discussed their implications on the physical processes. The modeling results show that the one-zone SSC model can successfully fit the SEDs of high-synchrotron-peaked BL Lacs (HBLs) and intermediate-synchrotron-peaked BL Lacs (IBLs), but fails to explain the SEDs of low-synchrotron-peaked BL Lacs (LBLs). The statistical analysis results for model parameters are summarized as follows. (1) No correlation is found between magnetic field (B) and the broken energy of relativistic electrons distribution (γ'_b) for HBLs and IBLs, but there are inverse correlations between γ'_b and the radius of emitting blob (R'_b) as well as the electrons number K'_e for HBLs and IBLs. It's therefore concluded that the variation of γ'_b is mainly caused by that of R'_b rather than B for HBLs and IBLs. (2) The Poynting flux in jets can not account for the observed radiations since the power in Poynting flux is smaller than the radiative power, and the cold protons could be the primary energy carrier in the jets.

Key words: galaxies: BL Lacertae objects – galaxies: active – galaxies: jets – radiation mechanisms: non-thermal

1 INTRODUCTION

The observed emissions from blazars are dominated by the non-thermal emissions from relativistic jets. Their spectral energy distributions (SEDs) are characterized by two distinct bumps: the first bump located at low-energy band is dominated by the synchrotron emission of relativistic electrons, and the second bump located at high-energy band could be produced by inverse Compton (IC) scattering (e.g., Böttcher 2007). The seed photons for IC process could be from the local synchrotron radiation of the same relativistic electrons (i.e. synchrotron self-Compton (SSC); e.g., Rees 1967; Maraschi et al. 1992; Tavecchio et al. 1998), or from the external photon fields (EC; e.g., Ghisellini & Tavecchio 2009; Dermer et al. 2009), such as those from accretion disk (e.g., Dermer & Schlickeiser 1993) and broad-line region (e.g., Sikora et al. 1994). The hadronic model is an alternative explanation for the high energy emissions from blazars (e.g., Mannheim 1993; Mücke et al. 2003; Dimitrakoudis et al. 2012; Dermer et al. 2012).

Blazars are traditionally divided into BL Lac objects (BL Lacs) and flat spectrum radio quasars (FSRQs) based on the emission line equivalent width (EW) being smaller

or larger than 5\AA . In general, the SEDs of BL Lacs having weak lines or absent lines can be reproduced well by the homogenous one-zone SSC model (e.g., Zhang et al. 2012), and the EC components are needed to explain the observed high energy radiation from FSRQs (e.g., Ghisellini et al. 2010, 2011; Yan et al. 2012a). However, it should be kept in mind that it seems that the one-zone SSC model sometimes fails to explain the gamma-ray emissions of several intermediate-synchrotron-peaked BL Lacs (IBLs; e.g., Abdo et al. 2011a) and low-synchrotron-peaked BL Lacs (LBLs; e.g., Abdo et al. 2011b), and even high-synchrotron peaked BL Lacs (HBLs; e.g., Aliu et al. 2012a).

The modeling of SED with a given radiation mechanism allow us to investigate the intrinsic physical properties of emitting region (e.g., Ghisellini et al. 1998; Ghisellini & Tavecchio 2008; Zhang et al. 2012; Yan et al. 2012a, 2013; Mankuzhiyil et al. 2011, 2012) and the physical conditions of jet (e.g., Celotti & Ghisellini 2008; Ghisellini et al. 2009, 2010, 2011), like the compositions, energy carrier and radiative efficiency of the jet. With a large number of blazars, Celotti & Ghisellini (2008) suggested that the jet should comprise a dominant proton component and only a small fraction of the jet power is radiated if there is one proton per relativistic electron. Ghisellini et al. (2011) found that there is a positive correlation between the jet

* E-mail: lizhang@ynu.edu.cn

power and the accretion disk luminosity for *Fermi* broad-line blazars, and confirmed that the jet should be protons dominated. In these previous studies, Ghisellini et al. (2009, 2010, 2011) mainly concerned the relation between the jet power and the accretion disk luminosity in *Fermi* blazars, which is more significant for FSRQs. Celotti & Ghisellini (2008) estimated the powers of blazars jets based on EGRET observations.

Since blazars show violent variability in multi-frequency bands, especially at the X-ray and gamma-ray bands, so the SEDs obtained simultaneously or quasi-simultaneously are crucial to reveal the physical properties of their jets. Moreover, to well constrain the model parameters and obtain the robust results for a given blazar, a high-quality SED with a good coverage is needed. Fortunately, Abdo et al. (2010) have assembled high-quality multi-wavelength data of 48 blazars in the first three months of the LAT sample (LAT Bright AGN Sample: LBAS) to build their quasi-simultaneous SEDs. The data from *Swift* were collected in one day, or several days; however, the *Fermi*-LAT data have been averaged over a period of three months. Therefore, the multi-frequency data are quasi-simultaneous, but not really simultaneous.

Because the SEDs of BL Lacs suffer less contamination of the emission from the accretion disk and EC process which always can be explained well by the one-zone SSC model, in order to reduce the uncertainties on the radiative mechanisms, we only consider BL Lacs here. In this work, we mainly take advantage of the quasi-simultaneous SEDs of BL Lacs having certain redshift reported in Abdo et al. (2010) to study the physical properties of their jets systematically within the frame of the simple one-zone SSC model. Moreover, we use the Levenberg-Marquardt (LM) method of χ^2 -minimization fitting procedure instead of the ‘‘eyeball’’ fitting to find the best-fit values of model parameters and their uncertainties. The cosmological parameters ($H_0, \Omega_m, \Omega_\Lambda$) = (70 km s⁻¹ Mpc⁻¹, 0.3, 0.7) are used throughout this paper.

2 MODELING FITTING PROCEDURE

The one-zone SSC assumes that non-thermal radiation is produced by both the synchrotron radiation and SSC process in a spherical blob filled with the uniform magnetic field (B), moving relativistically at a small angle to our line of sight, and the observed radiation is strongly boosted by a relativistic Doppler factor δ_D . The radius of emitting blob is $R'_b = \frac{t_{v,\min} \delta_D c}{1+z}$, where $t_{v,\min}$ is the minimum variability timescale. In this study, we assume a broken power-law electron energy distribution in the blob, and use the relativistic electron distribution given by Dermer et al. (2009), i.e.,

$$N'_e(\gamma') = K'_e H(\gamma'; \gamma'_{\min}, \gamma'_{\max}) \{ \gamma'^{-p_1} \exp(-\gamma'/\gamma'_b) \\ \times H[(p_2 - p_1)\gamma'_b - \gamma'] + [(p_2 - p_1)\gamma'_b]^{p_2 - p_1} \gamma'^{-p_2} \\ \times \exp(p_1 - p_2) H[\gamma' - (p_2 - p_1)\gamma'_b] \}, \quad (1)$$

where K'_e is the normalization factor, γ' is the Lorentz factor of a relativistic electron with rest mass m_e , and c is the speed of light. $H(x; x_1, x_2)$ is the Heaviside function: $H(x; x_1, x_2) = 1$ for $x_1 \leq x \leq x_2$ and $H(x; x_1, x_2) = 0$ everywhere else; as well as $H(x) = 0$ for $x < 0$ and $H(x) = 1$ for $x \geq 0$. The minimum and maximum energies of electrons

in the blob are γ'_{\min} and γ'_{\max} , respectively. This spectrum is smoothly connected with indices p_1 and p_2 below and above the electron’s break energy γ'_b . Here, quantities in the observer’s frame are unprimed, and quantities in the comoving frame are primed. Note that the magnetic field B is defined in the comoving frame, despite being unprimed.

For a given BL Lac with the electron energy distribution given by Eq. (1), the local non-thermal spectra is

$$f_\epsilon^{\text{tot}} = f_\epsilon^{\text{syn}} + f_\epsilon^{\text{SSC}}. \quad (2)$$

In the right hand of Eq. (2), the first term represents the synchrotron spectrum, which can be given by Finke et al. (2008)

$$f_\epsilon^{\text{syn}} = \frac{\sqrt{3} \delta_D^4 \epsilon' e^3 B}{4\pi h d_L^2} \int_0^\infty d\gamma' N'_e(\gamma') R(x), \quad (3)$$

where e is the electron charge, B is the magnetic field strength, h is the Planck constant, d_L is the distance to the source with a redshift z , $\epsilon' = [h\nu(1+z)/m_e c^2]/\delta_D$ is synchrotron photons energy in the co-moving frame. In equation (3), $R(x) = (x/2) \int_0^\pi d\theta \sin \theta \int_{x/\sin \theta}^\infty dt K_{5/3}(t)$, where $x = 4\pi \epsilon' m_e^2 c^3 / 3e B h \gamma'^2$, θ is the angle between magnetic field and velocity of high energy electrons, and $K_{5/3}(t)$ is the modified Bessel function of order 5/3. Here we use an approximation for $R(x)$ given by Finke et al. (2008). The second term of the right hand of Eq. (2) represents the SSC spectrum and is for isotropic and homogeneous photon and electron distributions (e.g., Finke et al. 2008)

$$f_{\epsilon_s}^{\text{SSC}} = \frac{9}{16} \frac{(1+z)^2 \sigma_T \epsilon_s'^2}{\pi \delta_D^2 c^2 t_{v,\min}^2} \int_0^\infty d\epsilon' \frac{f_\epsilon^{\text{syn}}}{\epsilon'^3} \\ \times \int_{\gamma'_{\min}}^{\gamma'_{\max}} d\gamma' \frac{N'_e(\gamma')}{\gamma'^2} F_C(q', \Gamma'_e), \quad (4)$$

where σ_T is the Thomson cross section, $m_e c^2 \epsilon'_s = h\nu(1+z)/\delta_D$ is the energy of IC scattered photons in the co-moving frame, $F_C(q', \Gamma'_e) = 2q' \ln q' + (1+2q')(1-q') + \frac{q'^2 \Gamma_e'^2}{2(1+q' \Gamma_e')^2} (1-q')$, $q' = \frac{\epsilon'/\gamma'}{\Gamma_e'(1-\epsilon'/\gamma')}$, $\Gamma'_e = 4\epsilon' \gamma'$, and $\frac{1}{4\gamma'^2} \leq q' \leq 1$.

In this model, there are nine free parameters. Six of them specify the electron energy distribution ($K'_e, \gamma'_{\min}, \gamma'_b, \gamma'_{\max}, p_1, p_2$), and the other three ones describe the global properties of the emitting region (B, R'_b, δ_D). For a given BL Lac, we will calculate its non-thermal flux using Eq. (2) and fit the observed multi-wavelength data using the LM algorithm given by Press et al. (1992). Because the LM method requires the initial input values of the model parameters, at beginning we do a preliminary modeling to the SED for each object to guess the starting values for parameters. More details about the applications of the LM method can be found in Mankuzhiyil et al. (2011, 2012). However, it should be stressed that there may be caveats involved in applying the χ^2 fitting to the non-linear model such as the SSC model Andrae et al. (2010). As pointed out by Andrae et al. (2010), for the non-linear model the number of degrees of freedom is hard to determined, consequently the reduced χ^2 is not a good method for model assessment and model comparison no longer. Other methods are needed to make judgement of goodness of the fit and make model comparison (e.g., applying the Kolmogorov - Smirnov (K-S) test for normality of the residuals of the SED fits in Mankuzhiyil et al. (2011) and investigating the

convergence of the model parameter in Yan et al. (2013)). Nevertheless, minimising χ^2 is the correct thing in order to fit the model to the observed data (Andrae et al. 2010). In this work, the LM method is just used to obtain the best-fit model parameters and their uncertainties. The uncertainties returned by LM method is the approximated symmetrical (standard) errors (the square root of the covariance matrix diagonal elements) of the model parameters, which depend on a quadratic approximation to the χ^2 -surface around the minimum (Press et al. 1992; Mankuzhiyil et al. 2011).

The low energy cutoff in electrons distribution γ'_{\min} is always poorly constrained by the SED modeling. In this study, in order to avoid overproducing the radio flux we set $\gamma'_{\min} = 500$ for Mrk 421 and BL Lac and $\gamma'_{\min} = 200$ for S5 0716+714, PKS 0851+202, GB6 J1058+5628 as well as ON 231 (W comae), and $\gamma'_{\min} = 100$ for the rest of objects.

3 APPLICATIONS

We compile the broadband SEDs covering from radio, optical, X-ray to GeV-TeV band from Abdo et al. (2010); Giommi et al. (2012) and the literature listed in TeV-Cat¹ for 22 BL Lacs having known redshift, including 10 HBLs, 6 IBLs and 6 LBLs (according to the classification of Ackermann et al. (2011)). The sources having bad *Fermi* data (only having flux upper limits) in Giommi et al. (2012) and other literature are also excluded here, although they maybe have the good optical-UV and X-ray data. The quasi-simultaneous SEDs including GeV-TeV data of Mrk 421, Mrk 501, PKS 2155-304, PKS 0447-439, 1ES 0414+009, RBS 0413, 1ES 1215+303 and B3 2247+381 are taken from Abdo et al. (2011c), Abdo et al. (2011d), Aharonian et al. (2009), Prandini et al. (2012), Aliu et al. (2012a), Aliu et al. (2012b), Aleksić et al. (2012a) and Aleksić et al. (2012b), respectively. The optical-UV data of PKS 0426-380 and 4C 01.28 are taken from Giommi et al. (2012). The rest of SEDs are taken from Abdo et al. (2010). The Plank data taken from Giommi et al. (2012) are plotted as square.

We apply our model fitting procedure to the SEDs of 22 *Fermi* BL Lacs. The extragalactic background light (EBL) model of Franceschini et al. (2008) is used to correct the absorption affect. The SEDs of our sources, together with the best-fit one-zone SSC SEDs, are shown in Figures 1–3. The best-fit model parameters are listed in Table 1. It can be found that in general the SEDs of 16 *Fermi* HBLs and IBLs covering from optical to GeV-TeV band are fit well by the simple one-zone SSC model (see Figures. 1–2 and Table 1) and most of their parameters are well constrained, except for HBL 1ES 0414+009 and IBL PG 1246+586. It seems that more complex model is needed for 1ES 0414+009 (e.g., Aliu et al. 2012a). The first three months average *Fermi* spectrum of IBL PG 1246+586 turns upward above 5 GeV, and is not a simple power-law, which evidently can not be explained by the simple one-zone SSC model. However, its one-year and two-year *Fermi* spectrum is featureless power-law². Hence, we do not think it needs more explanations of

the turning upward spectrum in this study. However, the fits to the SEDs of 6 LBLs are bad and we cannot obtain their meaningful best-fit values (see Figures 3 and Table 1).

4 RESULTS AND DISCUSSION

As mentioned above, this model includes nine parameters, in which six parameters are used to determine the electron energy distribution and the others are used to describe the global properties of the emitting region. Using the above best-fit values of the model parameters (note that γ_{\min} is assumed above) listed in Table 1, we can make a statistical analysis on the electron energy distribution and the properties of the emitting region. Because the model parameters of LBLs are poorly constrained, the following statistical analysis are focused on HBLs and IBLs.

4.1 Relativistic electron distributions

It can be seen that HBLs have distinctly greater γ'_b than IBLs (see Table 1). For the relativistic electrons spectral indexes (Figure 4), it can be found that the values of p_2 cluster around 3.8, while the values of p_1 distribute in a large range (1.4–2.2). Our results show that the values of $(p_2 - p_1)$ are in the range (1.0–3.0), typically around 2.0. It is interesting that several IBLs have $p_1 < 1.6$ and $(p_2 - p_1) > 2.0$, which may imply some clues on the acceleration process in the jet of a blazar (e.g., Summerlin & Baring 2012).

4.2 The physical conditions of emitting regions

From Table 1, it can be found that the derived values of magnetic field in the emitting regions are in the range (0.01–0.1) G, which are smaller than the results derived by Ghisellini et al. (2011); Zhang et al. (2012), and the values of δ_D are in the range (20–40), which are consistent with the results based on the observations (Savolainen et al. 2010). According to the SSC model, there would be relationships between δ_D and B for a given BL Lac, for example, $B\delta_D \propto [\nu_s^2/\nu_C](1+z)$ in the Thomson regime and $B/\delta_D \propto [\nu_s/\nu_C^2]/(1+z)$ in the Klein-Nishina (KN) regime, where ν_s and ν_C are the peak frequencies of the synchrotron radiation and the inverse Compton scattering. We have plotted the change of δ_B with B in Figure 5 and not found any correlations between B and δ_D . The lack of correlations may be due to the fact that the synchrotron peaks of these objects distribute in a large range.

The obtained minimum variability timescales vary from 1 hour to ~ 100 hours (see Table 1), and the corresponding radiuses of emitting blobs are in the range $(0.3–20) \times 10^{16}$ cm, which are consistent with that of TeV BL Lacs derived by Zhang et al. (2012).

4.3 Physical conditions of emitting regions vs. relativistic electron distributions

In the SSC model, $\gamma'_b \propto [B\delta]^{-1/2}\nu_s^{1/2}$, which shows that there is a relationship between γ'_b and B , i.e., $\gamma'_b \propto B^{-1/2}$ if ν_s and δ_D roughly keep constant. On the other hand, the static electron distribution we used could be considered as a solution to the electron continuity equation. Such

¹ <http://tevcat.uchicago.edu/>

² <http://tool.asdc.asi.it>

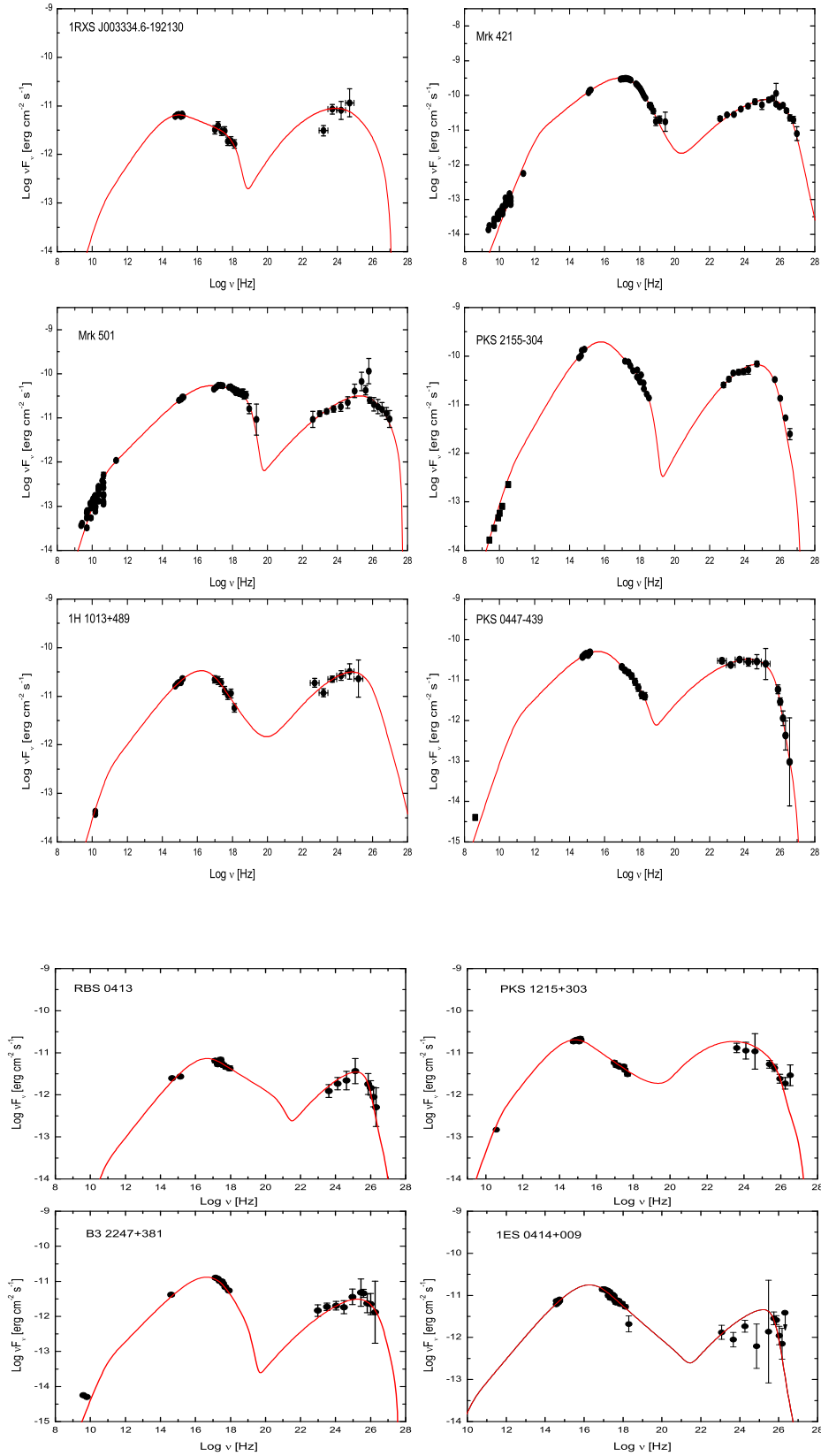


Figure 1. Best-fit one-zone SSC modeling for the observed SEDs of HBLs.

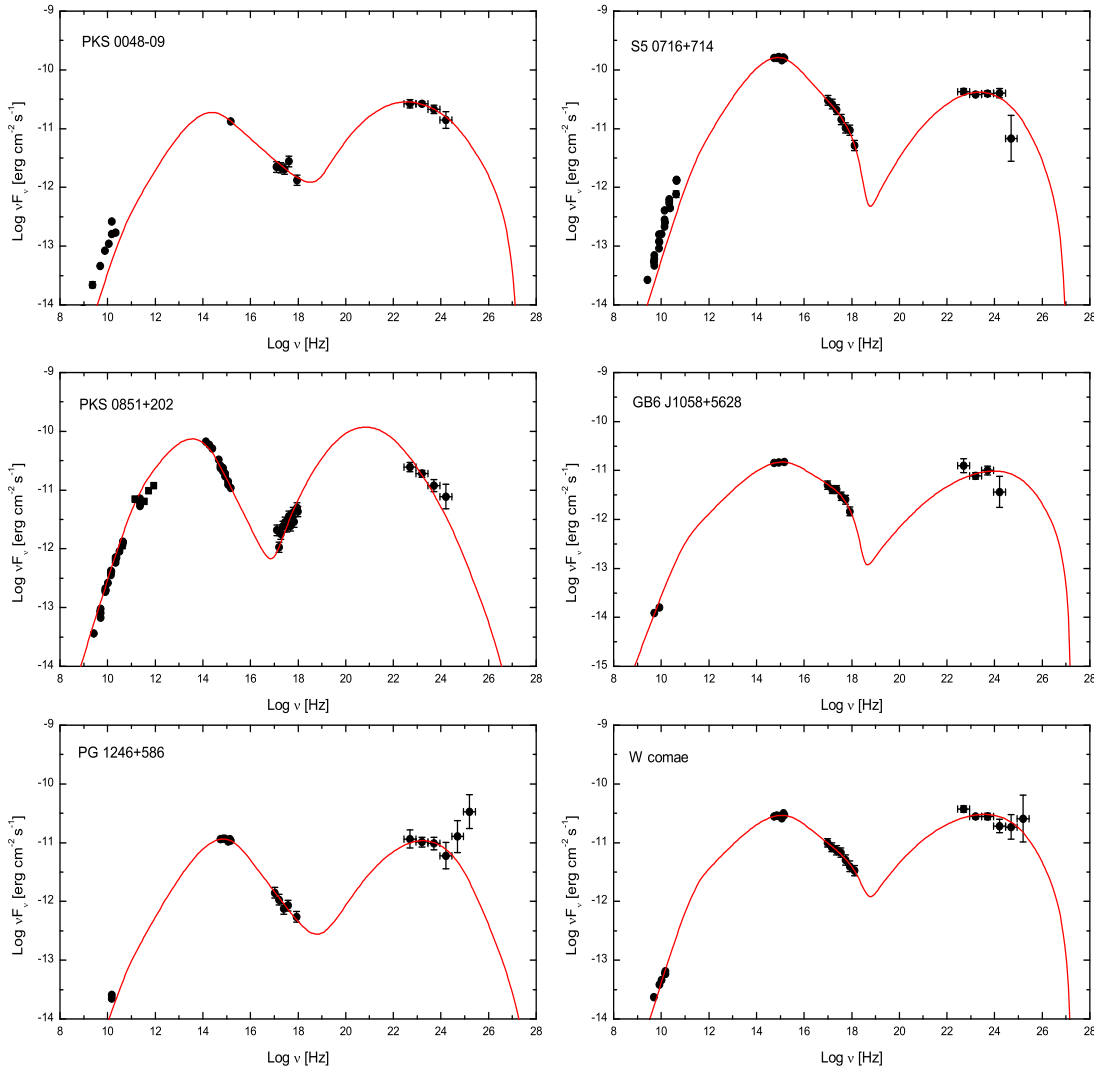


Figure 2. Same as in Figure 1, but for IBLs.

a continuity equation includes a injection term, a escape term, and a cooling term (synchrotron + SSC cooling), the continuous injection is balanced by the cooling and escape (Chiaberge & Ghisellini 1999; Li & Kusunose 2000; Böttcher & Chiang 2002; Tramacere et al. 2011; Yan et al. 2012b). Hence γ'_b is obtained when the cooling time $t_{\text{cool}} = 3m_e c^2 / [4\sigma_T c \gamma' (U'_B + U'_{\text{syn}})]$ is equal to the escape time $\eta R'_b / c$, where U'_{syn} is the synchrotron photon field energy density for IC scattering and $U'_B = B^2 / 8\pi$ is the energy density of magnetic field and η is a constant. Therefore, we have

$$\gamma'_b \propto 1 / [(U'_B + U'_{\text{syn}}) \eta R'_b]. \quad (5)$$

It is clear that γ'_b relies on the cooling process ($U'_{\text{syn}} + U'_B$) and the escape process $\eta R'_b$.

In Figures 1-2, it can be roughly estimated that the ratio of the SSC peak flux to the synchrotron peak flux is less than unity for HBLs and IBLs, which implies that $U'_B / U'_{\text{syn}} > 1$ and the synchrotron cooling is more important than SSC

cooling. Therefore, the relation $\gamma'_b \propto B^{-2}$ would be expected for HBLs and IBLs. However, no correlation between B and γ'_b is found in our sample (Figure 6), which may be caused by the fact that the change of γ'_b is not caused by the change of B .

On the other hand, if γ'_b mainly depends on the escape, the relation $\gamma'_b \propto R'^{-1}_b$ would be expected (Eq.5). In Figure 7, we show the distribution of γ'_b vs. R'_b . The errors of R'_b are estimated by using a Monte-Carlo method. The error weights are considered in the correlation analysis. It is interesting that an anti-correlation is found between γ'_b and R'_b , i.e., $\gamma'_b \propto 1/[R'_b]^{1.24 \pm 0.22}$ for HBLs and IBLs with the correlation coefficient $r = -0.82$ and a chance probability $p = 1.21 \times 10^{-4}$ (Figure 7). If the change of γ'_b is caused by the escape process, γ'_b should decrease with increase of K'_e . It's found that γ'_b does inversely correlate with K'_e with $r = -0.57$ and $p = 0.01$ (Figure 8). The anti-correlations between γ'_b and R'_b , K'_e found in our results indicate that for HBLs and IBLs γ'_b is mainly determined by the escape.

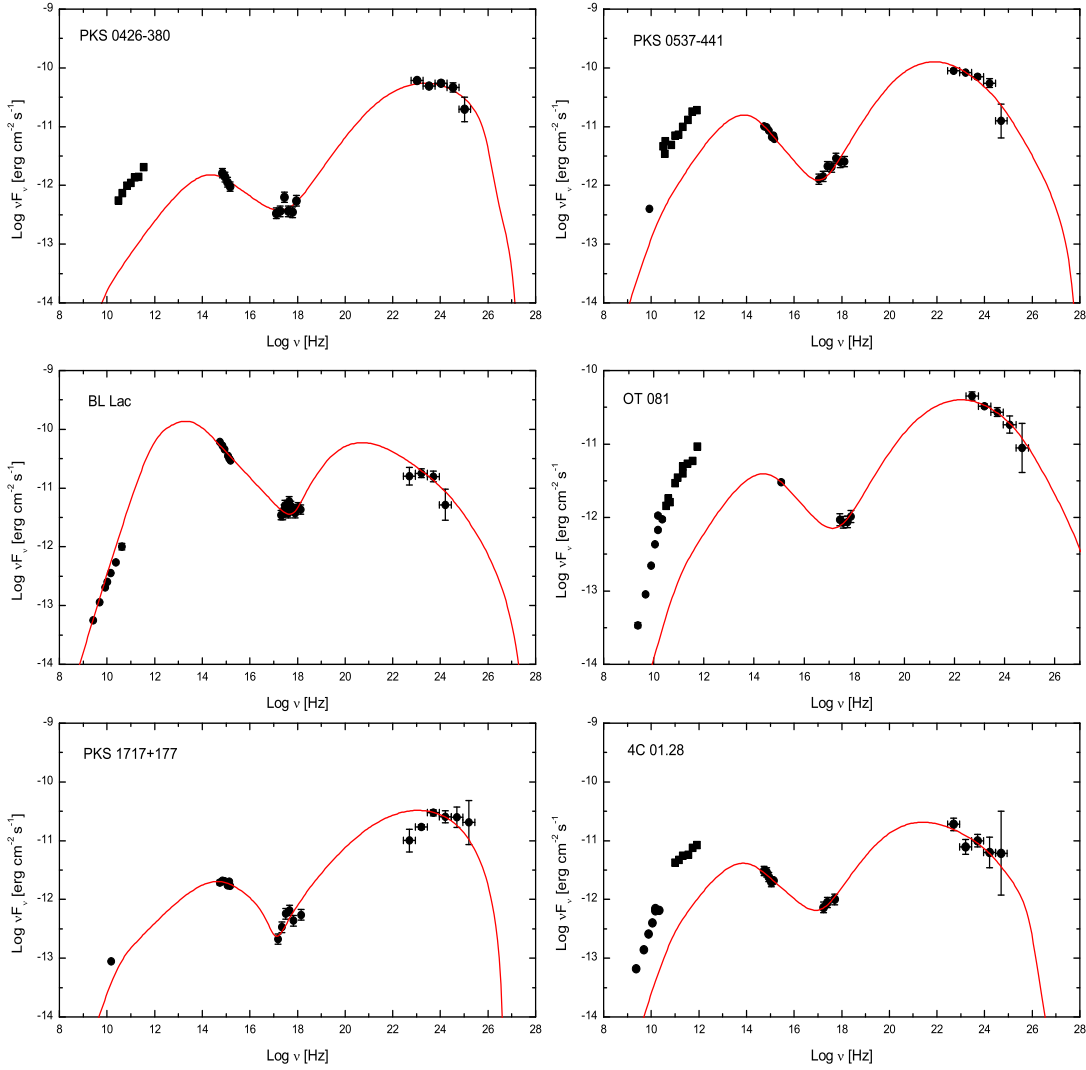


Figure 3. Same as in Figure 1, but for LBLs.

Moreover, as discussed above, no inverse and quadratic correlations between γ'_b and B for HBLs and IBLs also support that the change of γ'_b is mainly caused by that of the escape instead of B . However, the exact relationship between γ'_b and K'_e can not be determined by the current sample. To achieve it, larger sample with better covered SEDs are required.

4.4 The physical properties of jets

After obtaining the values of model parameters, we can estimate jet power and radiative power. The jet power (P_{jet}) is the sum of Poynting flux power (P_B) and the powers of relativistic electrons (P_e) and protons (P_p), i. e., $P_j = P_B + P_e + P_p$ in the stationary frame of the host galaxy, which are calculated as (Celotti & Fabian 1993; Celotti & Ghisellini 2008)

$$P_i = \pi R_b'^2 \Gamma^2 U_i' c, \quad (6)$$

where U_i' ($i = e, B, p$) are the energy densities associated with the emitting electrons U_e' , magnetic field U_B' , and protons U_p' in the comoving frame, respectively. We calculate U_p' by assuming one proton per emitting electron, then $U_p' = U_e'(m_p/m_e)/\langle\gamma'\rangle$ (Celotti & Ghisellini 2008), where $\langle\gamma'\rangle = \frac{\int N'_e(\gamma')\gamma' d\gamma'}{\int N'_e(\gamma') d\gamma'}$ is the average energy of relativistic electrons. Here, we take the bulk Lorentz factor $\Gamma = \delta_D$. On the other hand, for the radiative power, the energy density can be expressed as $U_r' = L'/(\pi R_b'^2 c)$, so it reads (Celotti & Ghisellini 2008)

$$P_r = L' \Gamma^2 \approx L \frac{\Gamma^2}{\delta_D^4}, \quad (7)$$

where L is total non-thermal luminosity.

It should be pointed out that the estimate of the proton kinetic power and relativistic electron's power are dependent on the value of γ'_{min} , which however is historically poorly constrained by the modelling, especially for low-power BL Lacs (e.g., Celotti & Ghisellini 2008). Due to the

Table 1. The best-fit model parameters and the reduced χ^2 . The first nine sources are HBLs, the second six sources are IBLs, and the third six sources are LBLs.

Name	B (0.01 G)	δ_D (10)	$t_{v,\min}$ (10^5 s)	γ'_{\max} (10^7)	γ'_b (10^4)	K'_e (10^{55})	p_1	p_2	χ^2_{red}
0033-1921	4.06 ± 1.24	2.43 ± 0.17	2.48 ± 1.21	0.07 ± 0.01	1.62 ± 0.20	0.12 ± 0.01	1.83 ± 0.08	3.29 ± 0.05	1.14
0414+009	1.30 ± 0.58	2.96 ± 1.36	3.54 ± 4.31	1.49 ± 2.70	12.67 ± 1.36	0.04 ± 0.02	1.88 ± 0.10	3.82 ± 0.07	3.96
0447-439	5.47 ± 1.38	3.63 ± 0.08	0.43 ± 0.11	0.052 ± 0.002	3.18 ± 0.29	0.05 ± 0.02	2.07 ± 0.03	3.96 ± 0.17	0.70
1013+489	5.72 ± 0.75	2.75 ± 0.47	0.55 ± 0.22	0.08 ± 0.04	6.82 ± 0.74	0.03 ± 0.01	2.03 ± 0.04	4.06 ± 0.19	2.11
2155-304	4.89 ± 0.66	1.97 ± 0.06	3.47 ± 0.52	0.087 ± 0.004	3.57 ± 0.20	0.011 ± 0.002	1.68 ± 0.02	3.79 ± 0.08	2.48
Mrk 421	4.23 ± 0.41	2.71 ± 0.27	0.42 ± 0.10	3.73 ± 0.81	18.43 ± 0.79	0.012 ± 0.002	2.13 ± 0.02	5.04 ± 0.18	1.39
Mrk 501	2.77 ± 0.63	2.99 ± 0.70	0.16 ± 0.11	0.16 ± 0.03	15.81 ± 3.10	0.007 ± 0.006	2.19 ± 0.09	3.12 ± 0.04	1.29
RBS 0413	5.48 ± 1.57	2.60 ± 0.55	0.23 ± 0.11	1.29 ± 0.42	9.97 ± 1.26	0.0014 ± 0.0006	1.93 ± 0.07	3.52 ± 0.34	1.91
1215+303	3.49 ± 0.17	3.58 ± 0.10	0.22 ± 0.02	0.27 ± 0.01	1.13 ± 0.04	0.0031 ± 0.0001	1.78 ± 0.01	3.61 ± 0.04	1.99
2247+381	5.45 ± 1.64	3.62 ± 0.05	0.14 ± 0.05	0.10 ± 0.06	8.87 ± 1.96	0.0004 ± 0.0002	1.96 ± 0.06	4.58 ± 0.42	0.54
0048-09	6.50 ± 5.84	2.50 ± 0.28	2.19 ± 1.74	0.10 ± 0.02	0.52 ± 0.04	0.015 ± 0.002	1.42 ± 0.18	3.72 ± 0.08	2.90
0716+714	5.90 ± 1.23	2.71 ± 0.47	3.51 ± 1.21	0.04 ± 0.01	0.92 ± 0.10	0.010 ± 0.002	1.49 ± 0.04	3.88 ± 0.07	1.98
0851+202	4.05 ± 2.41	2.40 ± 1.10	2.43 ± 3.34	0.14 ± 0.45	0.26 ± 0.10	0.13 ± 0.12	1.46 ± 0.40	4.65 ± 0.16	1.49
1058+5628	2.20 ± 1.14	2.40 ± 0.73	1.29 ± 0.72	0.06 ± 0.03	2.61 ± 0.30	0.06 ± 0.03	1.93 ± 0.05	3.59 ± 0.07	1.36
1246+586	8.82 ± 1.89	2.34 ± 0.34	3.06 ± 0.96	0.40 ± 0.02	0.89 ± 0.08	0.006 ± 0.006	1.43 ± 0.03	4.08 ± 0.08	1.52
W Comae	4.91 ± 0.12	2.70 ± 0.13	0.32 ± 0.04	0.06 ± 0.01	1.94 ± 0.09	0.046 ± 0.002	2.09 ± 0.02	3.65 ± 0.04	1.75
0426-380	1.08 ± 2.42	3.53 ± 4.01	0.93 ± 1.31	0.47 ± 0.02	1.77 ± 0.51	0.36 ± 0.78	1.78 ± 0.51	3.58 ± 0.93	2.41
0537-441	2.12 ± 1.55	3.62 ± 1.54	1.51 ± 1.38	0.38 ± 0.40	0.54 ± 0.09	0.20 ± 0.07	1.56 ± 0.13	3.96 ± 0.06	5.64
1717+177	1.79 ± 0.20	3.52 ± 0.18	0.036 ± 0.005	0.013 ± 0.003	1.79 ± 0.17	0.020 ± 0.001	2.12 ± 0.04	3.53 ± 0.19	3.97
BL Lac	1.86 ± 1.89	3.23 ± 1.70	0.95 ± 0.90	0.11 ± 0.09	0.29 ± 0.06	0.24 ± 0.04	1.84 ± 0.18	3.87 ± 0.04	4.10
OT 081	9.82 ± 9.80	2.31 ± 5.16	0.12 ± 0.55	2.00 ± 2.10	0.52 ± 0.58	0.007 ± 0.022	1.75 ± 0.66	3.76 ± 0.59	1.69
4C 01.28	10.56 ± 19.20	2.47 ± 3.42	0.66 ± 6.02	0.12 ± 0.43	0.30 ± 0.18	0.06 ± 0.13	1.69 ± 0.64	3.70 ± 0.32	0.96

Table 2. The ratios of the energy densities of relativistic electrons to magnetic fields in the emitting regions and the radiative powers, the jet powers in the forms of Poynting flux, bulk motion of electrons and protons (assuming one proton per emitting electron), as well as the redshifts of the sources.

Name	U'_e/U'_B	P_r (erg s $^{-1}$)	P_B (erg s $^{-1}$)	P_e (erg s $^{-1}$)	P_p (erg s $^{-1}$)	z
0033-1912	40.15	3.19×10^{44}	4.53×10^{43}	1.83×10^{45}	5.32×10^{45}	0.610
0414+009	14.79	4.24×10^{43}	2.28×10^{43}	4.85×10^{44}	9.62×10^{44}	0.287
0447-439	40.81	5.29×10^{43}	2.21×10^{43}	9.02×10^{44}	3.52×10^{45}	0.205
1013+489	37.60	7.25×10^{43}	1.33×10^{43}	5.00×10^{44}	1.61×10^{45}	0.212
2155-304	2.41	1.40×10^{44}	1.47×10^{44}	2.83×10^{44}	4.75×10^{44}	0.116
Mrk 421	14.54	7.42×10^{42}	5.43×10^{42}	7.89×10^{43}	6.65×10^{43}	0.031
Mrk 501	269.65	1.97×10^{42}	5.20×10^{41}	1.41×10^{44}	5.65×10^{44}	0.034
RBS 0413	28.13	1.13×10^{43}	3.36×10^{42}	9.48×10^{43}	2.24×10^{44}	0.190
1215+303	278.81	1.02×10^{43}	2.5×10^{42}	6.93×10^{44}	2.07×10^{45}	0.130
2247+381	23.64	2.67×10^{43}	2.63×10^{42}	6.10×10^{43}	1.64×10^{44}	0.130
0048-09	32.03	9.19×10^{44}	9.99×10^{43}	3.20×10^{45}	7.31×10^{45}	0.634
0716+714	1.81	3.47×10^{44}	5.07×10^{44}	9.19×10^{44}	1.23×10^{45}	0.26
0851+202	135.73	5.84×10^{44}	6.26×10^{43}	8.50×10^{45}	1.98×10^{46}	0.306
1058+5628	78.23	1.65×10^{43}	6.92×10^{42}	5.41×10^{44}	9.84×10^{44}	0.143
1246+586	6.40	8.54×10^{44}	2.08×10^{44}	1.33×10^{45}	2.36×10^{45}	0.847
W Comae	150.55	1.69×10^{43}	3.57×10^{42}	5.37×10^{44}	1.29×10^{45}	0.103
0426-380	5.42×10^4	2.55×10^{45}	7.45×10^{41}	4.04×10^{46}	1.05×10^{47}	1.111
0537-441	2344.32	3.20×10^{45}	1.70×10^{43}	3.89×10^{46}	1.08×10^{47}	0.892
1717+177	1.63×10^5	1.17×10^{43}	1.74×10^{40}	2.83×10^{45}	1.28×10^{46}	0.137
BL LAC	237.075	1.37×10^{43}	9.90×10^{42}	2.35×10^{45}	3.57×10^{45}	0.069
OT 081	2725.29	2.20×10^{44}	7.30×10^{41}	1.99×10^{45}	7.26×10^{45}	0.322
4C 01.28	369.50	1.31×10^{45}	1.62×10^{43}	5.98×10^{45}	2.44×10^{46}	0.888

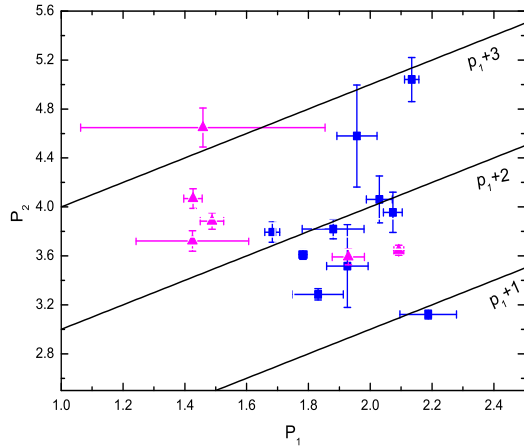


Figure 4. The relativistic electrons spectral indexes p_1 vs. p_2 . Squares: HBLs, triangles: IBLs.

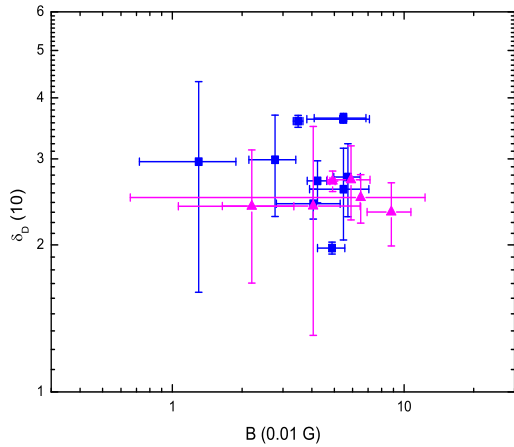


Figure 5. The Doppler factor δ_D as a function of B . The symbols are same as in Figure 4.

synchrotron self-absorption, the radio emission cannot be used to constrain the value of γ'_{\min} . However, the *Swift*-BAT observed hard X-ray data and *Fermi* GeV data at low energies could place constraints on γ'_{\min} in some degree. From our SED modeling results (Figures 1–3), it can be seen that the hard X-ray data and *Fermi* GeV data below 1 GeV can be fitted well. Therefore, we would like to believe that the jet kinetic powers we derived here are creditable.

Table 2 lists the ratios of the energy densities of relativistic electrons to magnetic fields in the emitting regions U'_e/U'_B , and the powers carried by the jets in the forms of radiations, Poynting flux, relativistic electrons and protons (assuming one proton per emitting electron).

From the results given by Table 2, we can see $P_e > P_B$ and $U'_e > U'_B$ in our sample, thus these jets are particle-dominated. In Figure 9, we show the changes of P_B , P_e , and P_p with radiative power P_r . It can be seen that $P_r > P_B$

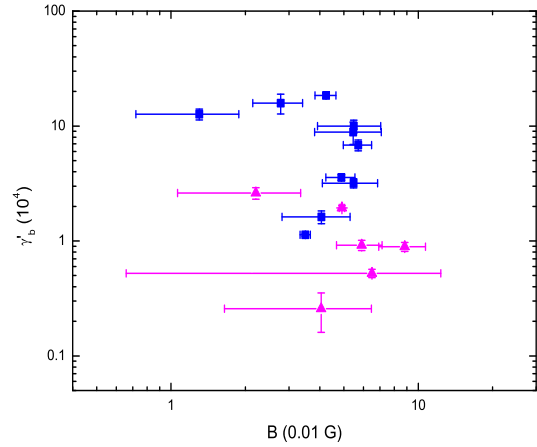


Figure 6. γ'_b as a function of B .

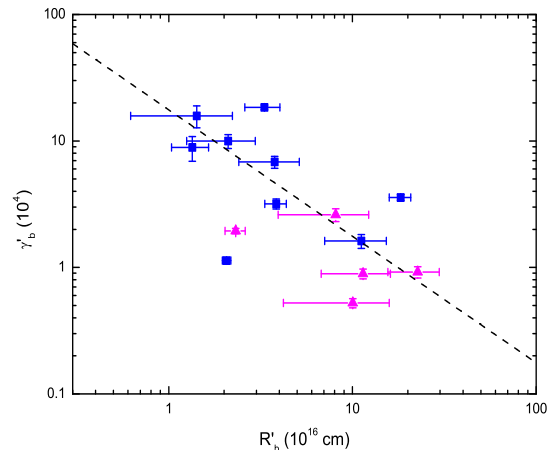


Figure 7. γ'_b as a function of R'_b . The dashed line represents the relationship $\gamma'_b \propto 1/[R'_b]^{1.0}$ for HBLs and IBLs.

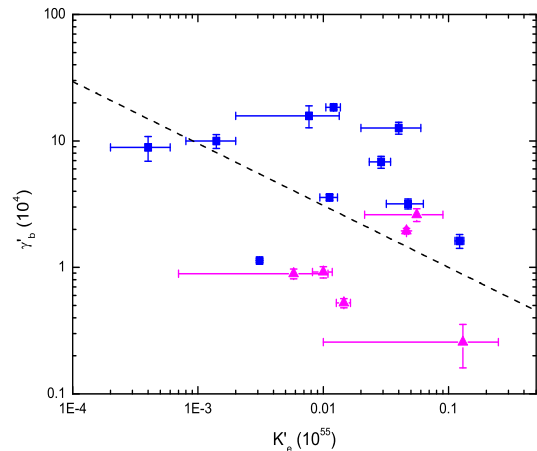


Figure 8. γ'_b as a function of K'_e . The dashed line represents the relationship $\gamma'_b \propto 1/[K'_e]^{0.49}$ for HBLs and IBLs.

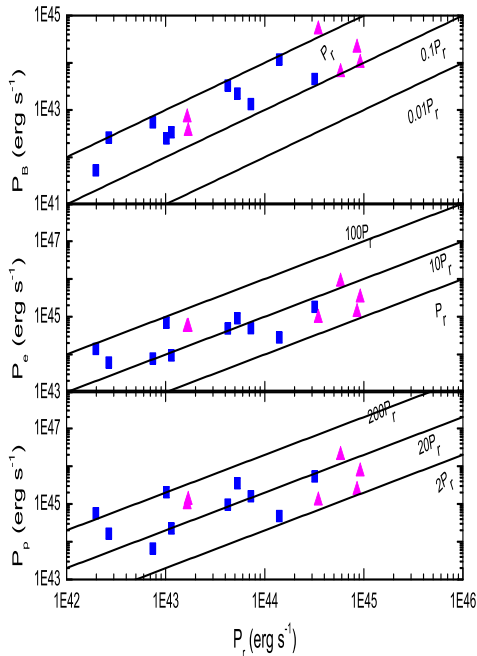


Figure 9. Powers in forms of Poynting flux, emitting electrons and bulk motion of cold protons as functions of the radiative output P_r .

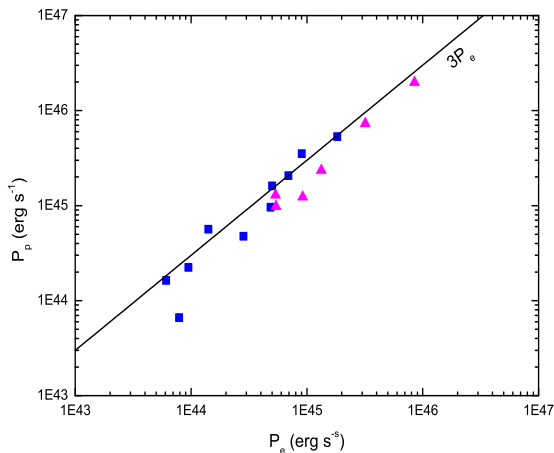


Figure 10. P_p as a function of P_e .

and $P_r/P_e \sim 0.01 - 0.8$. The former means that the Poynting flux cannot account for the observed radiation and the latter indicates that a large fraction of the relativistic electron power would be used to produce the observed radiation. Comparing middle panel with bottom panel in Figure 9, we can see $P_p > P_e$. In fact, we find $P_p \approx 3P_e$ in Figure 10. As mentioned above, it implies that only a small fraction of the jet power is dissipated into the observed radiation, $P_r/P_j \sim 1-30$ percent.

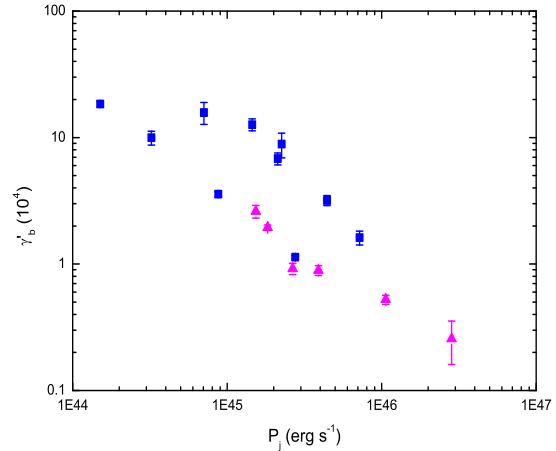


Figure 11. γ'_b versus P_j .

Furthermore, the relation $P_p \approx 3P_e$ in Figure 10 indicates that the average energy of relativistic electrons $\langle \gamma' \rangle \approx 610$, about one third of m_p/m_e , which may indicate that only a very small fraction $\eta_e \sim 1\%$ of the energy dissipated in the shock is picked up by the electrons, where $\eta_e = \frac{\langle \gamma' \rangle}{\Gamma} (m_e/m_p)$ (Giannios & Spitkovsky 2009) and $\Gamma = 25$ is used.

Compared to the result $P_r \sim P_e$ derived by Celotti & Ghisellini (2008), the relation $P_r < P_e$ derived here is due to the fact that our sample are the low power BL lacs. Due to the efficient cooling of electrons and the result we derived that P_r/P_e can be ~ 0.8 , it may be safe to suggest that an additional energy reservoir of cold hadrons is needed to accelerate electrons (e.g., Celotti & Ghisellini 2008).

4.5 The blazar sequence and implications on the differences between HBLs/IBLs and LBLs

Our results show that there is an anti-correlation between γ'_b and P_j for HBLs and IBLs, i.e., $\gamma'_b \propto P_j^{-(0.92 \pm 1.78)}$ with $r = -0.89$ and $p = 6.10 \times 10^{-6}$ (Figure 11). As mentioned in Celotti & Ghisellini (2008), this result is consistent with the prediction of the blazar sequence (Fossati et al. 1998; Ghisellini et al. 1998; Ghisellini & Tavecchio 2008) and is usually explained as that the radiative cooling is stronger in more powerful blazar. As we discussed above, it is the escape of relativistic electron which strongly affect the variation of γ'_b for HBLs and IBLs modeled here.

As mentioned in Section 3, the one-zone SSC model fails to fit the SEDs of LBLs. Furthermore, from Table 2 it can be found that LBLs have extreme values of U'_e/U'_B ($400-10^5$) in the frame of a one-zone SSC model. On the other hand, the simple one-zone SSC model predicts that the synchrotron emission peak frequencies of three LBLs (PKS 0426-380, PKS 1717+177, OT 081) are larger than 10^{14} Hz, which indicate that we overestimated the synchrotron peak frequencies in the SSC model. It is therefore suggested again that the one-zone SSC model is not the right model accounting for the multi-wavelength radiations from LBLs. With a large *Fermi* blazar sample, Fan et al. (2012) suggested that

the spectral index properties of LBLs are similar with that of FSRQs. Comparing Figure 3 with Figures 1 and 2, it can be found that the ratios of the Compton to the synchrotron peak energy fluxes of LBLs are greater than those of HBLs and IBLs, and then LBLs are Compton dominated. As suggested in Finke (2013), the Compton dominance is an more intrinsic indicator for blazar sequence.

5 CONCLUSIONS

We have modeled the quasi-simultaneous SEDs of 22 *Fermi* BL Lacs with a one-zone SSC model. We use a χ^2 -minimization procedure to obtain the best-fit model parameters and their errors, then the jet powers and the radiative powers are calculated.

Based on the derived results, we firstly discussed their implications on the physical processes in the emitting blobs. It can be found that there is no correlation between γ'_b and B . This lack of correlation was also found by Zhang et al. (2012) in a TeV BL Lacs sample and by Mankuzhiyil et al. (2012) in different states of Mrk 501. It seems that this lack of correlation is common in BL Lacs especially in HBLs and IBLs. Moreover, It can be found from our results that γ'_b is inversely correlated with R'_b as well as K'_e for HBLs and IBLs. These results indicate that in the emitting blobs of HBLs/IBLs where the synchrotron cooling is more important than IC cooling, γ'_b is mainly determined by the escape process.

Secondly, we concerned the powers of the *Fermi* BL Lacs jets. Our results confirm that the jet is energetically dominated by the proton component and only a small fraction of the jet power is transformed into radiation if there is one proton for a emitting electron (e.g., Celotti & Ghisellini 2008). Moreover, based on the physical properties of relativistic jets, our results confirm that HBLs/IBLs are different from LBLs again (e.g., Fan et al. 2012).

ACKNOWLEDGMENTS

We thank the anonymous referee for helpful comments. We thank P. Giommi, D. Paneque, D. Sentürk, A. Smith and E. Lindfors for sending us some data sets we used here. We acknowledge the support of Yunnan University's Science Foundation for graduate students under grant No. YNUY201260 and the Science Foundation for graduate students of Provincial Education Department of Yunnan under grant No. 2013J071. This work is partially supported by the Science Foundation of Yunnan Province under a grant 2009 OC.

REFERENCES

- Abdo A., A., et al., 2010, ApJ, 716, 30
 Abdo A. A., Ackermann M., Ajello M., et al. 2011a, ApJ, 726, 43
 Abdo A. A., Ackermann M., Ajello M., et al. 2011b, ApJ, 730, 101
 Abdo, A. A., Ackermann, M., Ajello, M., et al. 2011c, ApJ, 736, 131
 Abdo, A. A., Ackermann, M., Ajello, M., et al. 2011d, ApJ, 727, 129
 Ackermann M., et al., 2011, ApJ, 743, 171
 Aharonian F., et al. (H.E.S.S. Collaboration) 2009, ApJ, 696, L150
 Aleksić, J., et al. 2012a, A&A, 544, 142
 Aleksić, J., et al. 2012b, A&A, 539, 118
 Aliu E., et al. 2012a, ApJ, 755, 118
 Aliu E., et al. 2012b, ApJ, 750, 94
 Andrae R., Schulze-Hartung T., & Melchior P. 2010, arXiv:1012.3754
 Böttcher M. & Chiang J. 2002, ApJ, 581, 127
 Böttcher M. 2007, Ap&SS, 309, 95
 Celotti A., & Fabian A. C. 1993, MNRAS, 264, 228
 Celotti A., & Ghisellini G. 2008, MNRAS, 385, 283
 Chiaberge M. & Ghisellini G. 1999, MNRAS, 306, 551
 Dermer C. D., & Schlickeiser R. 1993, ApJ, 416, 458
 Dermer C. D., Finke, J. D., Krug H., & Böttcher M. 2009, ApJ, 692, 32
 Dermer C. D., Murase K., Takami H. 2012, ApJ, 755, 147
 Dimitrakoudis S., Mastichiadis A., Protheroe R. J., Reimer A. 2012, A&A, 546, A120
 Fan J. H., Yang J. H., Yuan Y. H., Wang J., Gao Y. 2012, ApJ, 761, 125
 Finke J. D., Dermer C. D., & Böttcher, M. 2008, ApJ, 686, 181
 Finke J. D. 2013, ApJ, 763, 134
 Fossati G., Maraschi L., Celotti A., Comastri A., Ghisellini G. 1998, MNRAS, 299, 433
 Franceschini A., Rodighiero G., & Vaccari M. 2008, A&A, 487, 837
 Giannios D. & Spitkovsky A. 2009, MNRAS, 400, 330
 Ghisellini G., Celotti A., Fossati G., Maraschi L., Comastri, A. 1998, MNRAS, 301, 451
 Ghisellini G. & Tavecchio F. 2008, MNRAS, 387, 1669
 Ghisellini G. & Tavecchio F. 2009, MNRAS, 397, 985
 Ghisellini G., Tavecchio F., Ghirlanda G. 2009, MNRAS, 399, 2041
 Ghisellini G., Tavecchio F., Foschini L., Ghirlanda G., Maraschi L., Celotti, A. 2010, MNRAS, 402, 497
 Ghisellini G., Tavecchio F., Foschini L., Ghirlanda G. 2011, MNRAS, 414, 2674
 Giommi, P. et al. 2012, A&A, 541, 160
 Jones, F. C. 1968, Phys. Rev., 167, 1159
 Kirk J. G., Rieger, F. M., Mastichiadis, A. 1998, A&A, 333, 452
 Li H., & Kusunose M. 2000, ApJ, 536, 729
 Mannheim, K., 1993, A&A, 269, 67
 Maraschi, L., Ghisellini, G., & Celotti, A. 1992, ApJL, 397, L5
 Mankuzhiyil N., Ansoldi S., Persic M., & Tavecchio F. 2011, ApJ, 733, 14
 Mankuzhiyil N., Ansoldi S., Persic M. et al. 2012, ApJ, 753, 154
 Mücke, A., Protheroe, R. J., Engel, R. et al. 2003, APh, 18, 593
 Prandini E., Bonnoli G., Tavecchio F. 2012, A&A, 543, 111
 Press W.H., et al. 1992, Numerical Recipes (Cambridge: Cambridge University Press)
 Rees M. J. 1967, MNRAS, 137, 429
 Savolainen T., Homan D. C., Hovatta T. et al., 2010, A&A, 512, 24

- Sikora M., Begelman M. C., & Rees M. J. 1994, ApJ, 421, 153
Summerlin E. J., & Baring M. G. 2012, ApJ, 745, 63
Tavecchio F., Maraschi L., Ghisellini G. 1998, ApJ, 509, 608
Tramacere A., Massaro E., Taylor A. M. 2011, ApJ, 739, 66
Yan D. H., Zeng H. D., Zhang L. 2012a, PASJ, 64, 80
Yan D. H., Zeng H. D., Zhang L. 2012b, MNRAS, 424, 2173
Yan D. H., Zhang L., Yuan Q., Fan Z. H., Zeng H. D. 2013, ApJ, 765, 122
Zhang J., Liang E. W., Zhang S. N., Bai J. M. 2012, ApJ, 752, 157